Aerodynamic Interactions in Formation Flight for Wake Vortex Surfing

Jia Cheng Chan[1], Henrik Hesse[2]
University of Glasgow Singapore, 537 Clementi Road, Singapore 599493

Peng Cheng Wang[3]
Singapore Institute of Technology, 10 Dover Drive, Singapore 138683

Formation flight typically observed in migratory birds allows the trailing aircraft to benefit from surfing the updraft of the wingtip vortices generated by a leading aircraft. This results in higher lift and reduced fuel consumption for the trailing aircraft. However, the formation spacing in longitudinal, lateral, and vertical direction directly impacts the aerodynamics performance of the trailing aircraft. This paper aims to utilize computational fluid dynamics (CFD) tool – OpenFOAM, to capture the wake vortex dynamics from the leading wing using URANS and LES turbulence models. The selected model is then utilized to explore the position of the trailing aircraft in formation and to determine the optimal spacing in terms of aerodynamic improvements in lift and drag.

I. Introduction

Despite Covid-19 severely disrupting the number of flights, Airbus [1] and Boeing [2] forecasted a 70% increase in both passenger and freight traffic in 2040 comparing to the pre-pandemic fleet number. This growth in air traffic will eventually leads to a more congested sky and a negative impact on climate change due to greenhouse gas emissions [3]. The challenges faced by the aviation industry to achieve sustainability require significant enhancements in fuel efficiency to minimize the emission of greenhouse gases. There are several passive and active ways to reduce the carbon emissions such as using sustainable aviation fuels [4], lighter materials for aircraft structures [5], more efficient engines [6] and optimizing the flight operations [7]. Wake vortex surfing [8, 9] is one of the envisioned solutions that utilizes the aerodynamics features of aircraft to improve the efficiency of flight operations and fuel consumptions, which helps in reducing the greenhouse gas emissions without making notable changes to the existing aircraft designs.

A classic example of vortex surfing is found in long-distance migratory birds. The flock is led by a strong head bird, followed by birds flying on both sides in a V-shaped formation. The upwash of the vortices generated from the wingtip of the leading bird creates additional lift force for the trailing birds and this mechanism is repeated by the successive birds and the formation is established [10]. This formation allows the migratory birds to travel additional mileage for the same amount of energy. With the inspiration from migratory birds, powered flight began to explore the possibilities of formation flight [11, 12, 13]. The updraft of the vortices produced by the wingtip of the leading aircraft causes a forward rotation of the lift vector to the trailing aircraft, resulting in a smaller angle of attack (α) and induced drag [14]. Thus, the trailing aircraft in the formation flight will utilize the whirlwinds of turbulence produced by leading aircraft to achieve a reduction in induced drag and hence better fuel flow savings. Wake vortex surfing is

---

[1] PhD Student, Aerospace Engineering, AIAA Student Member.
[2] Assistant Professor, Program Director, Aerospace Engineering, AIAA Member.
[3] Associate Professor, Engineering Cluster.

still at the very early stage to be commercialized and operationalized. The trailing aircraft must be positioned at the 'sweet spot' to optimize the aerodynamic effects from formation flight. This position is defined by the spacing to the leading aircraft in longitudinal (x), lateral (y) and vertical (z) direction, as shown in Figure 1.

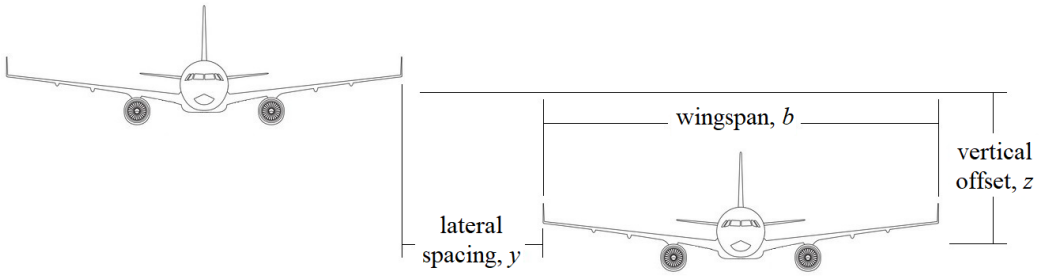

(a) Formation spacing in y-z plane.

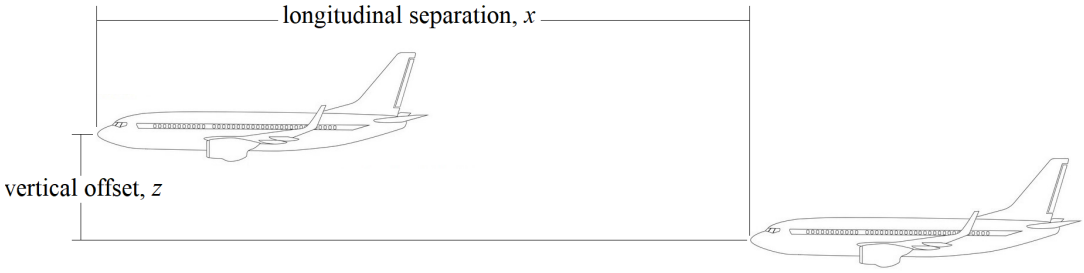

(b) Formation spacing in x-z plane.

Figure 1. Formation spacing overview.

Deutsche Forschungsanstalt für Luft- und Raumfahrt (DLR) [15], NASA [16], USAF Test Pilot School (TPS) [17] and Air Force Institute of Technology (AFIT) [18] have conducted the formation flight programs using their various fighter aircraft. The formation is in a proximity where x/b is between 3 and 4.2 and the trailing aircraft has achieved fuel saving of around 15% – 18%.

NASA and USAF [19] extended the use of vortex surfing to C-17 transport aircraft with a longitudinal spacing of 1,000 feet (x/b = 5.9) and 3,000 feet (x/b = 17.6), and different points in lateral and vertical position. Using the same aircraft type, USAF Research Lab (AFRL) and Defense Advanced Research Projects Agency (DARPA) established the renowned Surfing Aircraft Vortices for Energy (SAVE) program [20, 21] which use the same formation flight concept but increase the longitudinal spacing to 3,000 – 8,000 feet (x/b = 17.6 – 46.9). The fuel saving for the trailing C-17 is in the range of 5–10%.

Most recently, Airbus has conducted considerable efforts in passenger aircraft vortex surfing research named Wake Energy Retrieval (WER) [22] to reduce aviation emissions, as shown in Figure 2. The "fello'fly" flight demonstration [23, 24] involving two A350 aircraft was conducted flying from Toulouse, France to Montreal, Canada with a set of operations procedure as shown in Figure 2. The formation has longitudinal spacing of 9,000 – 12,000 feet (x/b = 42 – 57) and both lateral and vertical spacing of 50 – 100 feet. This project has saved more than six tons of carbon dioxide emissions, which is projected to be over 5% of fuel savings for long-haul flights.

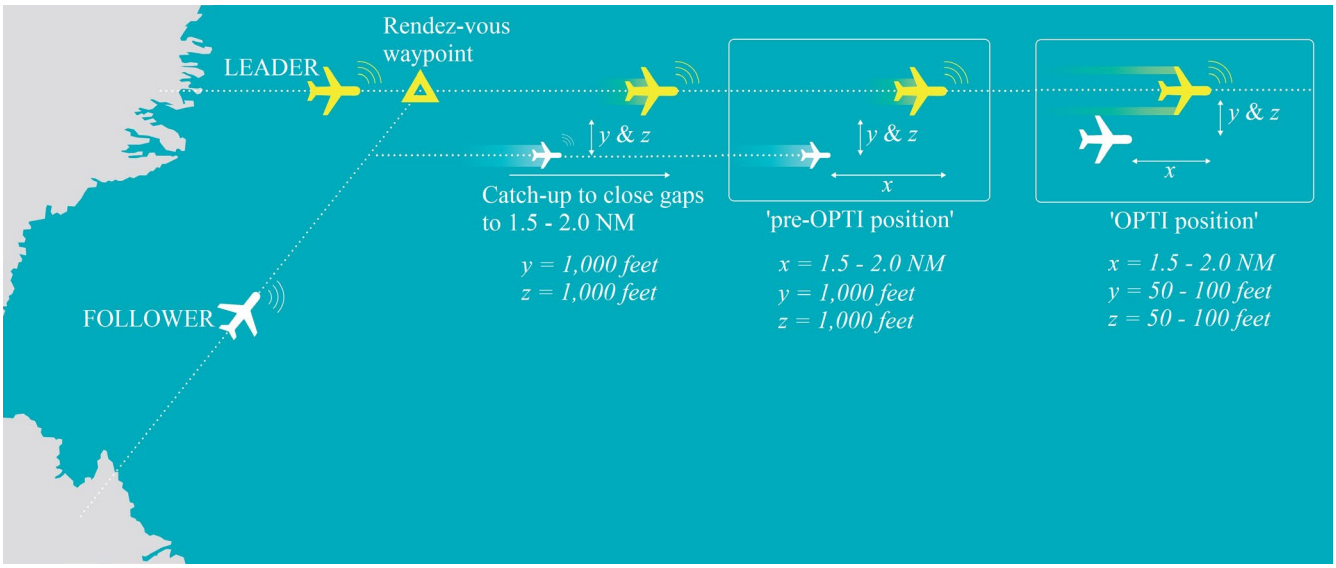

Figure 2. Airbus 'fello fly' concept of operations [23].

The economic and environmental benefits of vortex surfing are undoubted. As trailing aircraft is the beneficiary, its position in the formation must be determined and maintained during the vortex surfing phase to maximize the gains. Other than the flight test, several numerical simulations research [25-28] have been conducted over the last few decades to investigate the trailing aircraft position and its aerodynamics implications on vortex surfing. With the available data from SAVE program, Halaas et al. [25] used Reynolds-Averaged Navier Stokes (RANS) for the C-17 formation simulation, with consideration on the trim condition of following aircraft. The authors have validated the RANS simulation estimated mean values result against the actual flight test data with 95% confidence on the wake dynamics. Singh et al. [26] used a multi-fidelity CFD simulation on blended-wing-body UAVs in close tandem formation flight. The authors found that both the Vortex Lattice Method (VLM) and RANS turbulence models predict the same location of minimum drag and maximum lift, but RANS is more accurate in the lift and drag calculation, with a smaller deviation from the experimental results. Whereas Zhang et al. [27] used RANS to determine the optimal lateral spacing, vertical distance and the optimum formation of simplified tailless delta wing UAVs in the close formation flight. Vechtel et al. [28] used Large Eddy Simulation (LES) to generate vortex flow fields with small perturbations of the vortex lines, which is a more representative flow field for real flight conditions.

Based on the above literature, most of the CFD simulation for formation flight are carried out using RANS turbulence model. Generally, RANS is an appropriate model to achieve adequate solutions with higher computational efficiency. However, the predictive accuracy of RANS model often degrades [29] for downstream vortices or flows with substantial adverse pressure gradients. On the other hand, LES [30, 31] model which relies on the spatial filtering of turbulence energy, can reproduce the massive turbulence with a much higher accuracy and predict the vortex shedding and flow recirculation more accurately.

In this paper, the authors will first validate the performance of different unsteady RANS turbulence models as well as the LES model, on capturing the wingtip vortices. The more accurate model will be implemented when moving on to the wake vortex surfing cases to explore the aerodynamics effects on relative position of leading-trailing aircraft in formation. This research aims to capture the persistent vortex mechanism in the downstream and determine the optimal position of the leading-trailing wing in vortex surfing.

II.Methodology

The CFD approach [32, 33] appears to be very promising in the current state. It is relatively inexpensive, and the costs are expected to be lowered as the computers get more powerful. Furthermore, CFD allows to examine any location in the region of interest and interpret its performance through a set of thermal and flow parameters and it has

great control over the physical process. However, a validation work is still necessary before starting the research case to ensure the accuracy of the framework. The primary CFD research instrument used in this paper is OpenFOAM (Open-source Field Operation and Manipulation) [34] – a free, open source and one of the leading software for CFD. It has been used to successfully capture the vortices, or the wakes behind the airfoils [35, 36].

O'Regan et al. [37] presented the CFD model with vorticity confinement model to capture the trailing vortices generated by a symmetrical airfoil profile of NACA0012. The CFD model with additional forcing term aims to retain the vortex strength in the downstream. The results covered the normalized axial velocity, vortex trajectory, vortex size and vortex core center location at α = 10°. The literature also incorporates wind tunnel test data, which makes it a comprehensive source. The CFD validation in this paper is using the standard URANS and LES solvers without modification on the source code. The accuracy of the turbulence models in trailing vortices modelling will be assessed before implementing the appropriate framework on the formation flight.

A. Pre-processing

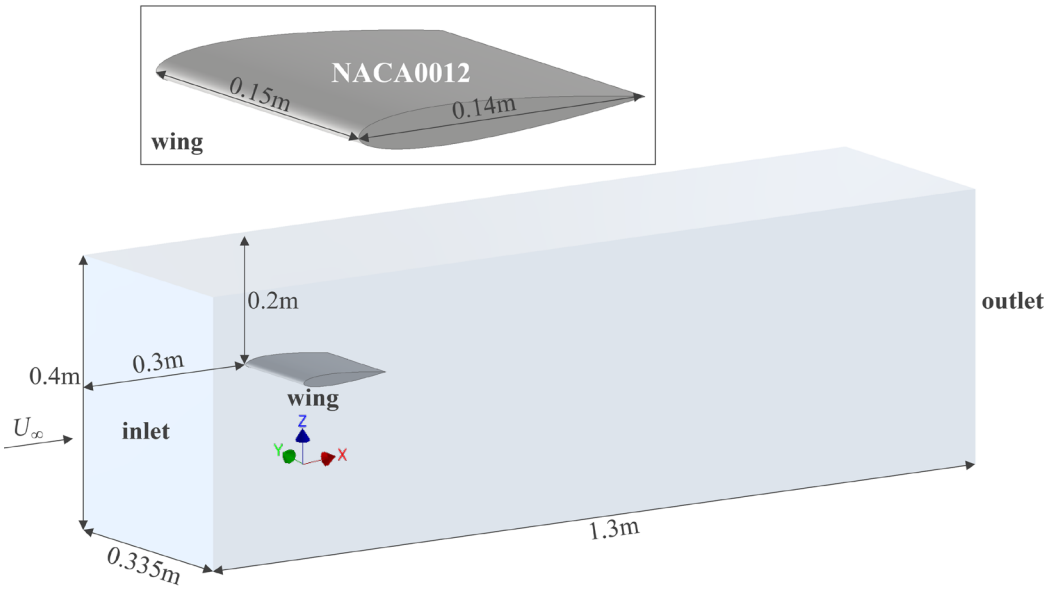

Figure 3. Wing model in domain for validation.

As illustrated in Figure 3, the wing geometry and boundary condition for the validation case is built to exactly the same as the literature [37], with chord of 0.14m and semispan of 0.15m. The simulation domain consists of an inlet with freestream velocity, $U_\infty = 34$ m/s which corresponds to chord-based Reynolds number, $Re_c = 3.25 \times 10^5$, an outlet of constant zero pressure, a symmetry plane at the wing root and the remaining walls of the domain are set as slip boundaries [38], which appoints zero shearing and no viscous effect on the surface. Whereas the wing geometry is no-slip boundary, to fix the velocity to zero and model the viscous layer on the surface.

The domain and geometry are further processed with blockMesh [39] and snappyHexMesh utility [40] for mesh generation in OpenFOAM. Considering the mesh convergence study by O'Regan et al. [37] and the computational resources, the meshing here produces 4.6×10^6 cells with 80% of the total mesh cell counts contained within the volume around the vortex, to achieve a satisfactory result. For such mesh size, time step of 1×10^{-5} is applied in the simulation to ensure the Courant number is below 1. The simulation run time also allows 20 chord-flow times over the wing model [41], where the flow field is observed to be stable.

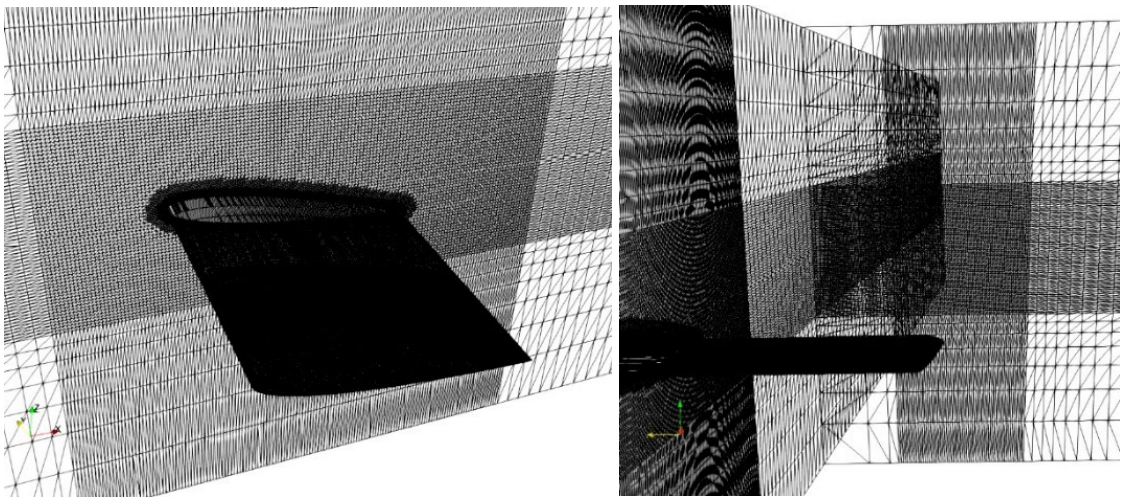

Figure 4. Mesh generation with snappyHexMesh.

B. Solving

Based on the validation case settings, pisoFoam [42] – an OpenFOAM transient solver for incompressible flow is chosen for the CFD simulation. The unsteady RANS turbulence models [43] that are commonly used such as Spalart-Allmaras (*S-A*), k-epsilon (*k-ε*) and k-omega shear stress transport (*k-ω SST*) are employed at the initial stage to determine the most appropriate turbulence model for wake vortex capturing. Besides URANS, the LES model [44] is also taking part in the validation effort. LES model is well known for its accuracy in predicting turbulent flow as it directly resolves the large eddies in the flow while models the small eddies through subgrid scale model.

1. URANS

Comparing the results of using different turbulence models as shown in Table 1, *k-ω SST* has showed the best prediction on the wake vortex dynamics.

Table 1. Comparison of wake vortex represented by different turbulence models.

	Maximum velocity component U_z, at x/c=0	Core axial velocity deficit, at x/c=0	Vortex core diameter along y-axis, at x/c=0
Exp. Fhp. (O'Regan et al.)	$0.5309U_\infty$	$0.7233U_\infty$	0.1149c
S-A	$0.2935U_\infty$	$0.8125U_\infty$	0.1316c
k-ε	$0.3374U_\infty$	$0.8051U_\infty$	0.1567c
k-ω SST	$0.4721U_\infty$	$0.8672U_\infty$	0.1149*c*

That is mainly attributed to the zonal formulation of the *k-ω SST* model [45], where the *k-ω* model is applied to model the near-wall region before gradually transforming to the *k-ε* model in the outer wake far-field. The damped cross-diffusion derivative term in the ω equation [46] is the essential component to modify the eddy viscosity formulation to account for the transport effects of the turbulent shear stress. This provides a more accurate flow field prediction, particularly for cases involving adverse pressure gradients and pressure-induced separations. The low Reynolds correction in the *SST* model also eliminates the requirement for an additional treatment for the viscosity affected wall region. The *SST* variant of the standard *k-ω* model has improved the accuracy and stability for the wake vortex simulation but with insignificantly longer computational run time. The transport equations for turbulence kinetic energy, k and specific dissipation rate, ω are as follows:

$$\frac{\partial k}{\partial t} + U_j \frac{\partial k}{\partial x_j} = P_k - \beta^* k\omega + \frac{\partial}{\partial x_j}\left[(\nu + \sigma_\omega \nu_t)\frac{\partial k}{\partial x_j}\right] \quad (1)$$

$$\frac{\partial \omega}{\partial t} + U_j \frac{\partial \omega}{\partial x_j} = \alpha S^2 - \beta \omega^2 + \frac{\partial}{\partial x_j}\left[(\nu + \sigma_\omega \nu_t)\frac{\partial \omega}{\partial x_j}\right] + 2(1 - F_1)\sigma_{\omega 2}\frac{1}{\omega}\frac{\partial k}{\partial x_i}\frac{\partial \omega}{\partial x_i} \quad (2)$$

where the blending function F_1 that distinguishes the boundary layer and freestream is given as:

$$F_1 = \tanh\left\{\left\{\min\left[\max\left(\frac{\sqrt{k}}{\beta^* \omega y}, \frac{500\nu}{y^2 \omega}\right), \frac{4\sigma_{\omega 2} k}{CD_{k\omega} y^2}\right]\right\}^4\right\} \quad (3)$$

$$CD_{k\omega} = \max\left(2\rho\sigma_{\omega 2}\frac{1}{\omega}\frac{\partial k}{\partial x_i}\frac{\partial \omega}{\partial x_i}, 10^{-10}\right) \quad (4)$$

and the turbulent viscosity, ν_t is calculated using equation below:

$$\nu_t = a_1 \frac{k}{\max(a_1 \omega, SF_2)} \quad (5)$$

$$F_2 = \tanh\left[\left[\max\left(\frac{2\sqrt{k}}{\beta^* \omega y}, \frac{500\nu}{y^2 \omega}\right)\right]^2\right] \quad (6)$$

The default value for the model coefficients in pisoFoam is listed in Table 2 below:

Table 2. Default model coefficient for the *k-ω SST* model.

β^*	σ_{k1}	$\sigma_{\omega 1}$	α_1	β_1	σ_{k2}	$\sigma_{\omega 2}$	α_2	β_2	a_1	b_1	c_1
0.09	0.85	0.5	5/9	3/40	1.0	0.856	0.44	0.0828	0.31	1.0	10.0

However, the vortices in this turbulence model are still dissipating too quickly. The maximum tangential velocity at *x/c*=3 location is only about 50% of the experimental data. To overcome the excessive vortex dissipation, Ahmad [47] used a very fine mesh resolution of $0.0021c$ at the vortex core region to resolve the wingtip vortices and its downstream projection. To reduce the computational consumption for the heavy mesh, O'Regan et al. [48] proposed to use adaptive mesh refinement method to further refine the mesh around the vortex core, or alternatively to use vorticity confinement model which introduces additional forcing terms in the momentum equations [49]. Kolomenskiy et al. [50] suggested a coupled RANS-LES model, where LES is used to solve the domain past the wing trailing edge due to its ability to explicitly resolve the turbulent scales in the flow.

2. LES

LES approach is more suitable for vortex shedding flow [51] as the numerical grid scale is spatially filtered by the governing equations. The LES solves the large-scale turbulence by the discretized equations, where these large eddies are significantly influenced by the geometric boundaries, and they contain most of the kinetic energy in the flow and more responsible for the transport of momentum, heat, and mass in the flow. Those filtered small-scale eddy motion which are less impactful yet computationally expensive are modelled through the subgrid scales (SGS) models. The most-used SGS model is the Smagorinsky model [52]. The momentum equation with the subgrid scale stress tensor, τ_{ij}^{sgs} from Smagorinsky model for LES [44] is as follows:

$$\frac{\partial \hat{\rho}\hat{u}_i}{\partial t} + \frac{\partial \hat{\rho}\hat{u}_i\hat{u}_j}{\partial \hat{x}_j} = -\frac{\partial \hat{p}}{\partial x_i} - \frac{\partial}{\partial x_j}\left(\tau_{ij} + \tau_{ij}^{sgs}\right) \quad (7)$$

where the SGS stress tensor τ_{ij}^{sgs} is to represent the effect of unresolved turbulence, with breakdown into anisotropic and isotropic parts:

$$\tau_{ij}^{sgs} = a_{ij}^{sgs} + \frac{2}{3}k_r \delta_{ij} \quad (8)$$

where the anisotropic component, a_{ij}^{sgs} is correlated with the Smagorinsky eddy viscosity, μ^{sgs} and the Smagorinsky constant, C_S which is taken as 0.18 here, is given as:

$$a_{ij}^{sgs} = -2\mu^{sgs}\widehat{S_{ij}} \quad (9)$$

$$\mu^{sgs} = \hat{\rho}(C_S\Delta)^2\sqrt{\widehat{S_{ij}}\widehat{S_{ij}}} \tag{10}$$

and the turbulent kinetic energy, k_r in the isotropic part of the SGS stress tensor is as follows:

$$k_r = \frac{1}{2}\tau_{ij}^{sgs} \tag{11}$$

With these constants and variables, the equation for the subgrid scale stress tensor is expressed as:

$$\tau_{ij}^{sgs} = 2\mu^{sgs}\widehat{S_{ij}} - \frac{2}{3}\hat{\rho}k_r\delta_{ij} \tag{12}$$

The isotropic part to be modelled only accounts for a relatively small amount of the overall energy in the flow field [53], which makes LES a more accurate model than the URANS. By refining the mesh grid, the subgrid scale region becomes smaller and lesser, which makes the LES model more accurate and approaching Direct Numerical Simulation. Before starting the LES in pisoFoam, a short simpleFoam RANS simulation using *k-ω SST* model is carried out to initialize the quasi-steady state flow dynamics. The aerodynamic fields are then mapped to the LES simulation as the starting conditions. Time step for the LES model here is 1×10^{-5} to keep the Courant number below 1.

C. Post-processing

The result is extracted to ParaView [54] for post-processing. The vortex core location is identified at where U_y and U_z are minimum, and thereafter the data across the vortex core at plane x/c = 0, 1, 2 and 3 are plotted for validation, as illustrated in Figure 5.

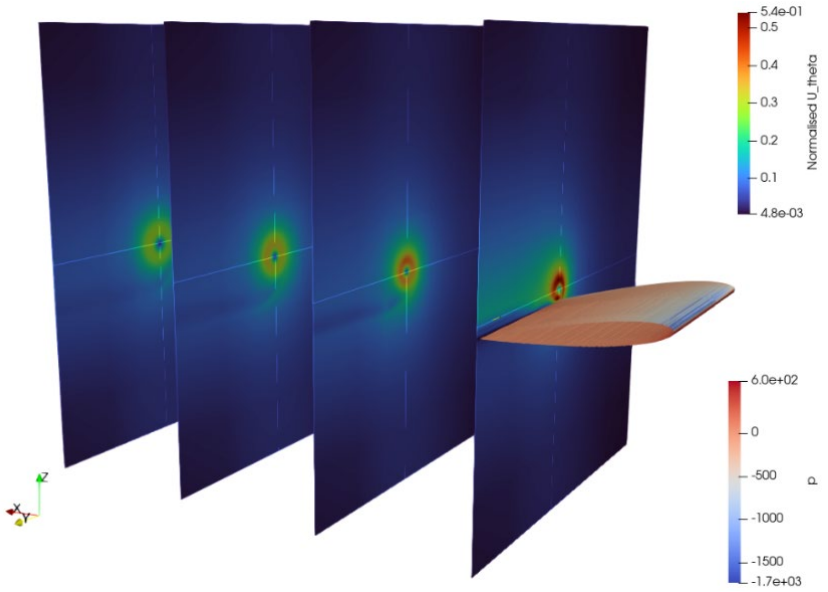

Figure 5. Plotting data across vortex core.

The validation of the URANS and LES model on the normalized tangential velocity across the vortex core are shown in Figure 6. The presence of wake vortex exhibited a V-shaped pattern in the graphs. The vortex core center location is represented by the valley of the V-shaped graph, where the tangential velocity is close to zero. The diameter of the vortex core is measured by taking the distance between the two tips, where the crossflow is at maximum. The tangential velocity is calculated from the resultant of velocity vectors in *y* and *z* axis, defined as $U_\theta = \sqrt{{U_y}^2 + {U_z}^2}$. This is one of the critical parameters in vortex capturing as it indicates the swirling motion or vortex form of the fluid.

D. Validating

From the results plotted in Figure 6, the LES did perform better than the URANS model as expected. Starting at *x/c*=0, the URANS is 13% below experimental data while LES is only 5%. As the vortices developed downstream, the rapid dissipation of URANS expanded the deviation to 48% and LES successfully improved it by 21%. In comparison, the URANS turbulence model with vorticity confinement correction from literature [37] has maintained an almost constant circulation throughout the *x/c*=0 to *x/c*=3, while the LES with the vorticity confinement is over-predicting. Therefore, the LES framework used here has adequately captured the wake vortex and maintained the downstream characteristics in the near field.

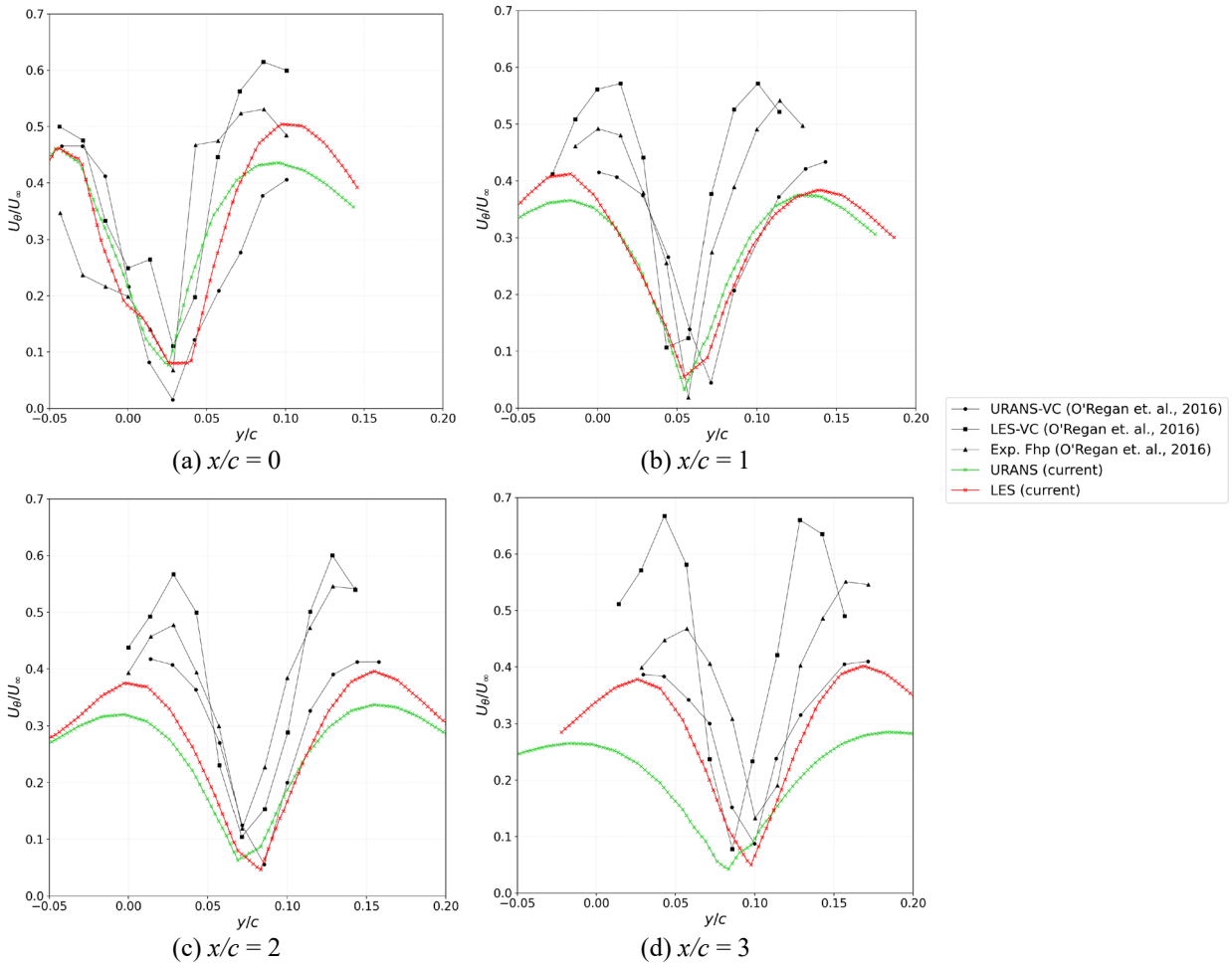

(a) *x/c* = 0 (b) *x/c* = 1

(c) *x/c* = 2 (d) *x/c* = 3

Figure 6. Normalized tangential velocity magnitude U_θ / U_∞ across the vortex core for α= 10°.

In addition to the tangential velocity, the axial velocity profiles around vortex core region are plotted in Figure 7. As the wingtip vortices roll up and rotate around the vortex core, the flow curls inwards to the vortex core center, resulting in axial velocity deficit [55]. The axial velocity deficit is one of the unsteady factors in vortices. It fluctuates at *x/c*=0 in all turbulence models as well as the experiment. As the vortices further developed downstream, the axial velocity component within the vortex core was stabilized to a more consistent deficit. In this study, both the URANS and LES models have showed the axial velocity deficit. Despite the slight over-prediction, the deficits have similar trends with the DNS and LES research [56] on the same topic. Again, the axial velocity deficit in the LES simulation is closer to the experiment data, as compared to URANS results.

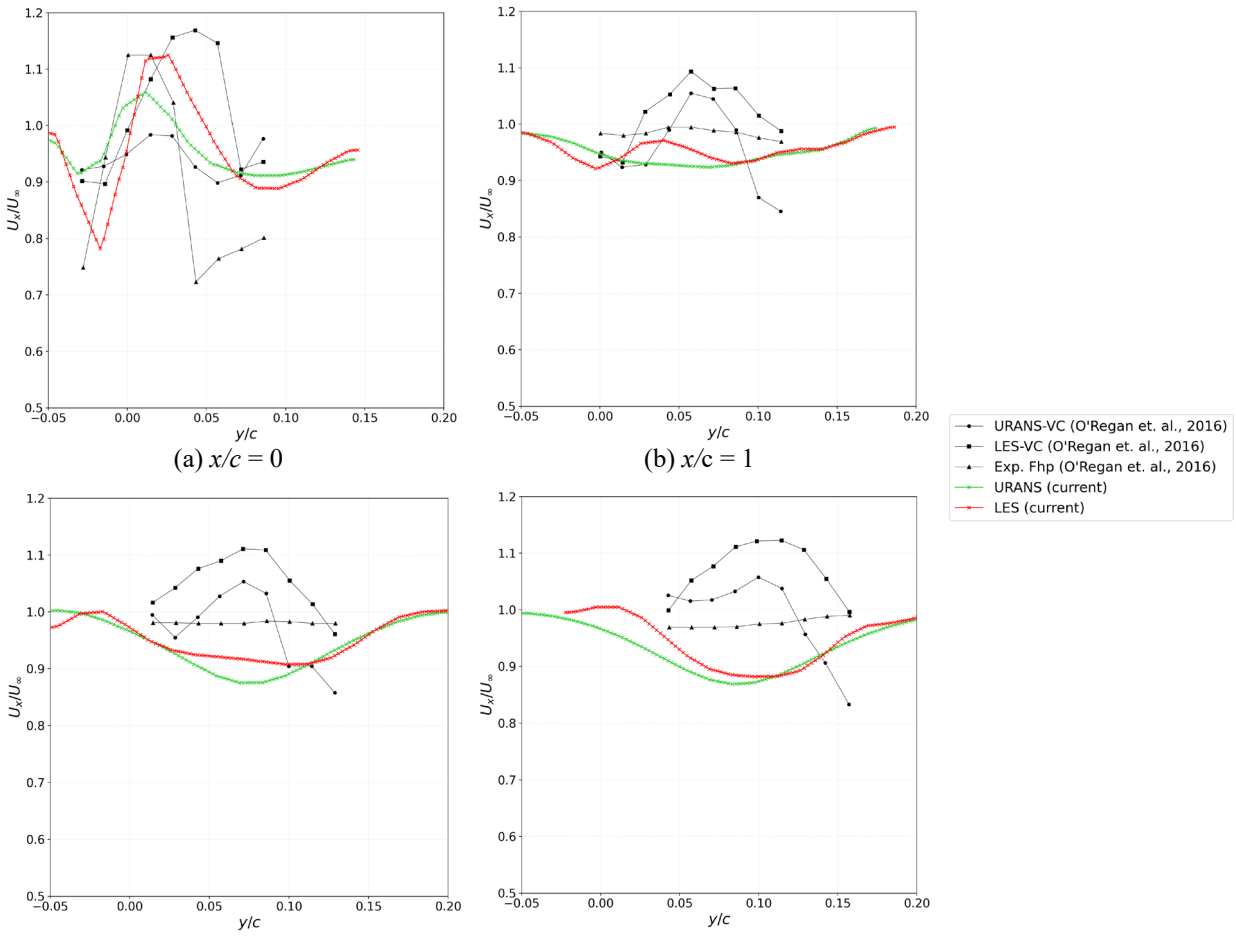

(a) $x/c = 0$ (b) $x/c = 1$

(c) $x/c = 2$ (d) $x/c = 3$

Figure 7. Normalized axial velocity U_x / U_∞ across the vortex core for α= 10°.

With the tangential velocity profile, the vortex core size can be easily defined by the distance of core center to the point of maximum tangential velocity. The vortex trajectory with the vortex core center and size are plotted in Figure 8. As the turbulence dissipates downstream, the vortex core diffuses and grows in radius. Both the URANS and LES have the core center location fairly accurately but LES performs better in computing the vortex core size. The overall trajectory of the vortex core is moving inboard and marginally downwards, which agreed to the experimental trajectory in Figure 8.

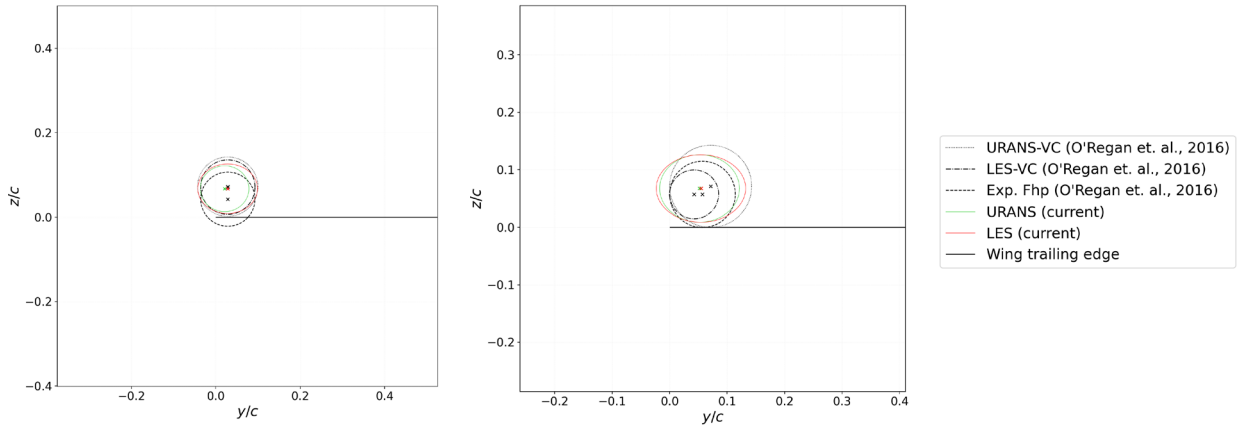

(a) x/c = 0 (b) x/c = 1

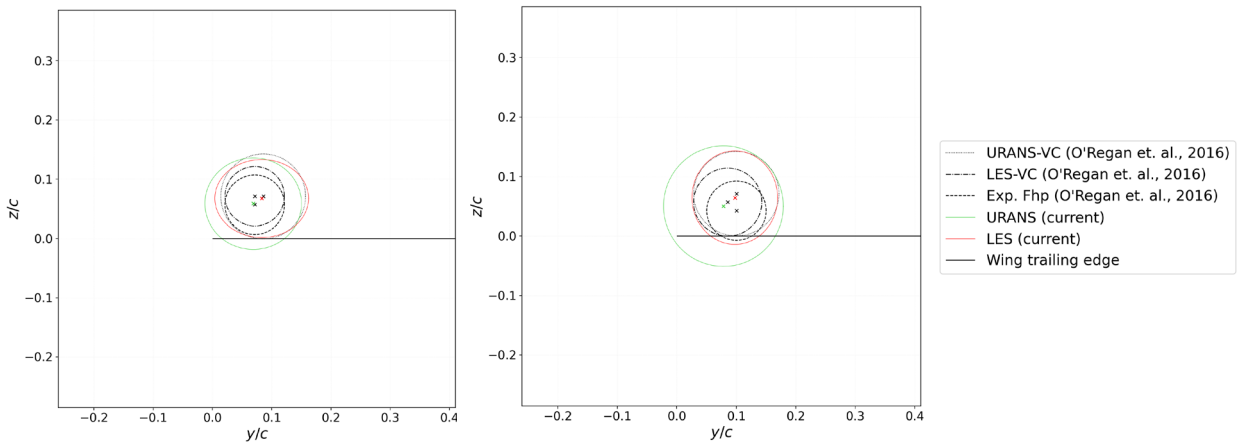

(c) x/c = 2 (d) x/c = 3

Figure 8. Downstream development of vortex trajectory, size, and core center location for α= 10°.

It is clear from the validation work discussed above that LES has a greater level of accuracy in predicting the wake vortex physics. It is superior in capturing the turbulence and maintaining the wingtip vortices behavior in the near field. Thus, it is chosen for the simulation on formation flight. To examine the benefit from the wake vortex surfing, aerodynamic coefficients such as lift and drag coefficients are the quantitative parameters. Hence, it is necessary to validate against another literature to ensure the turbulence model is estimating it correctly. Martínez-Aranda et al. [57] has conducted a wind tunnel experiment on rectangular NACA0012 wing with chord length, c=0.1m, aspect ratio, AR=2 and Reynold's number, $Re = 1.33 \times 10^5$. From Figure 9, it can be seen that the lift coefficient is matching well with the literature, but underpredicted the drag coefficients for α below 12°.

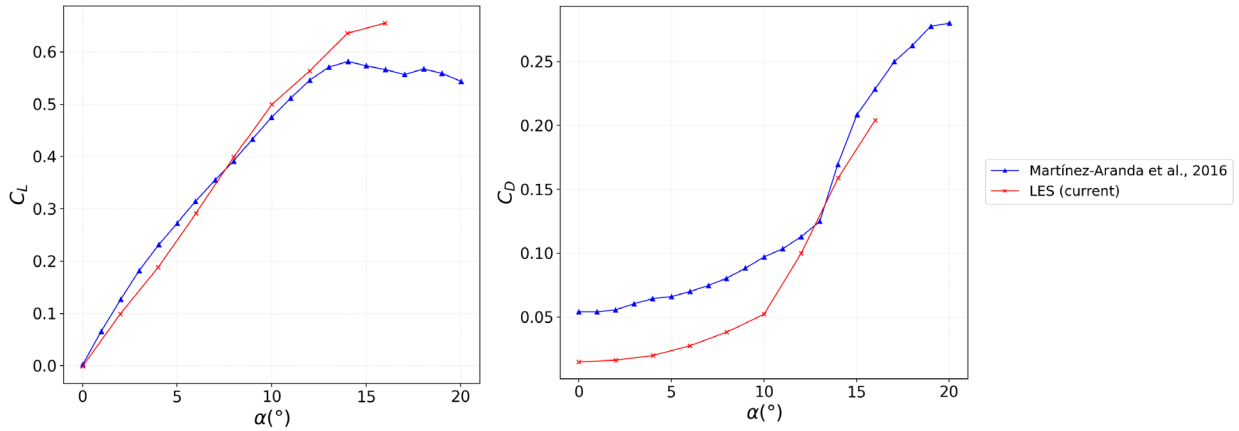

(a) Lift coefficient validation (b) Drag coefficient validation

Figure 9. Aerodynamics coefficient validation.

III. Formation Flight

In the formation simulation, the same LES model in pisoFoam is used for the analysis. The wing with α=10° used during the validation is put in place as the leading wing in the formation modelling. Another wing of the same NACA0012 airfoil profile with chord, c=0.14m and wingspan, b=0.3m, at α=0°, is placed at the trailing position as shown in Figure 10.

Before the formation flight simulation, a preliminary simulation on the solo flight of trailing wing itself is first conducted to gather the initial aerodynamic data. Any changes in the aerodynamic performance when it is in the

formation flight is correlated to the effect of the wake vortices induced by the leading wing and considered as the vortex surfing effect.

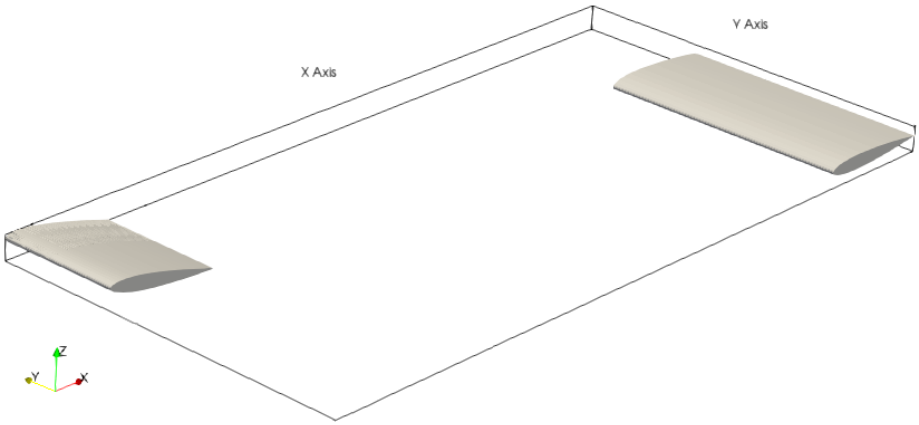

Figure 10. Leading and trailing wings in formation.

As the wingtip vortices behavior in the near field ($x/b < 3$) remains nearly constant [37, 58], the impact of vortex surfing on the trailing wing along the longitudinal axis is minimal in the close formation [59]. However, due to the slight degradation of the vortex in the LES model shown in validation work above, a simulation will be carried out for trailing wing to be positioned at different longitudinal separation (x/b) from the leading wing while having zero wingtip spacing in lateral and vertical axis (y/b=0, z/b=0) for the maximum benefits according to Lissaman and Shollenberger's theory [60]. Thereafter, the trailing wing will be placed on the fixed x/b plane but in various lateral and vertical spacing. Figure 11 below is illustrating the wake vortex surfing with trailing wing at x/b=2.

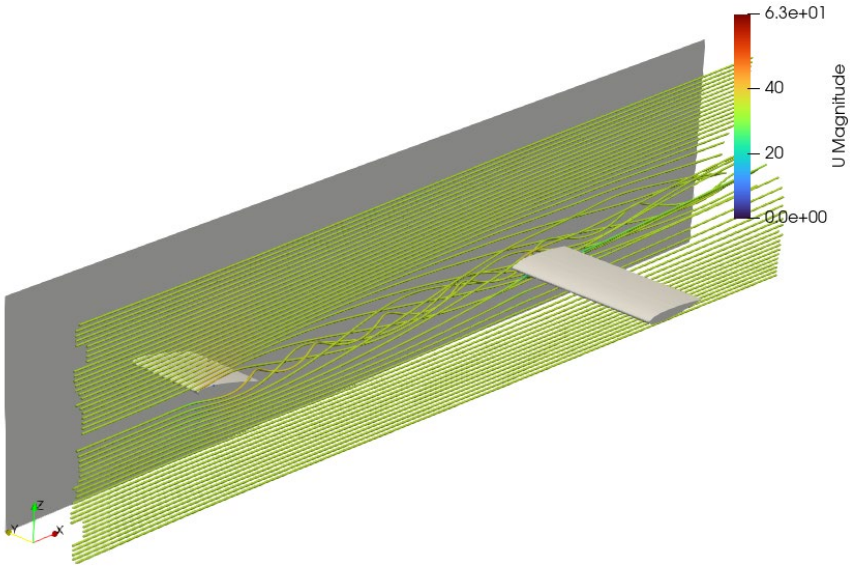

Figure 11. Stream tracer on wingtip vortices in formation.

IV.Results

The CFD results on the aerodynamic coefficients against different longitudinal separation, x/b is shown in Figure 12. In the close formation flight, it can be observed that the leading wing with α = 10° does not experience any noticeable change in terms of the lift and drag characteristics, as compared to solo flight. The trailing wing with a symmetrical airfoil profile and α = 0° is having approximately zero lift coefficient when it is flying individually. When flying in the formation, the trailing wing is however benefiting tremendously from the wake surfing effect.

Stating with variation on the *x*-axis separation and maintaining $y/b = 0$ and $z/b = 0$, the aerodynamic benefit on the trailing wing decreases slightly as it moves further downstream. This is due to the loss of vortex strength as energy dissipates over time, but the drop in benefits along the longitudinal separation is rather negligible in comparison to the gains made.

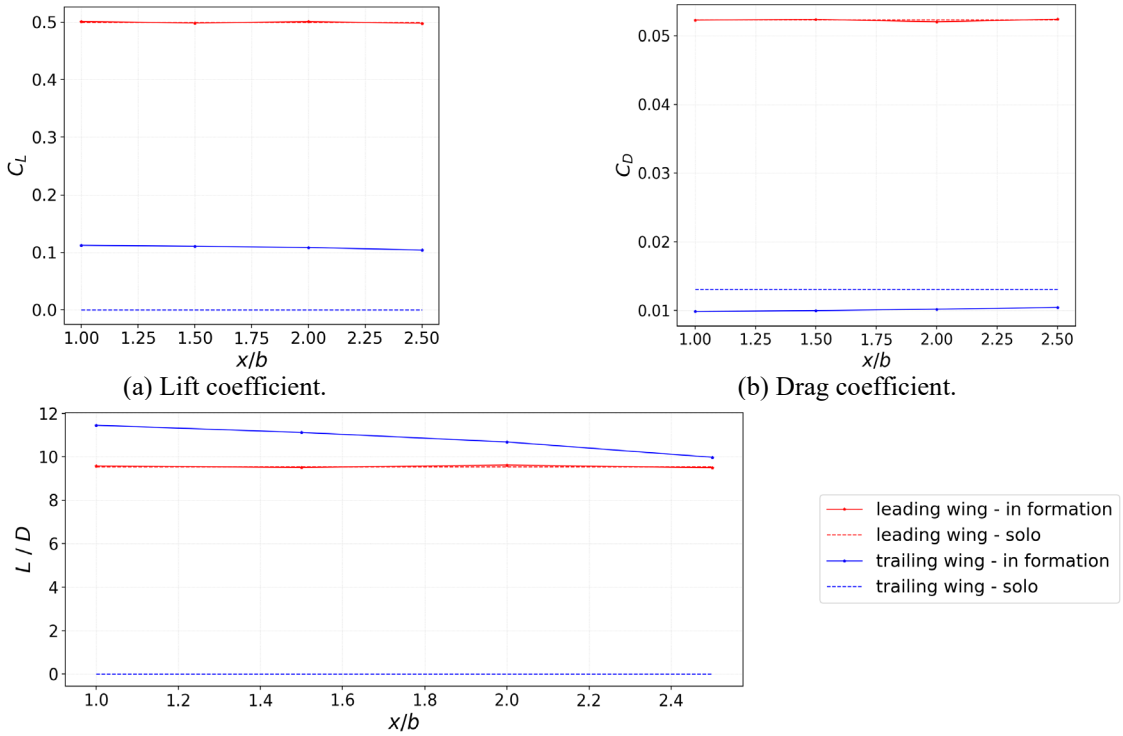

(a) Lift coefficient.

(b) Drag coefficient.

(c) Lift-to-drag ratio

Figure 12. Aerodynamics performance against longitudinal separation in formation.

Based on Hummel's findings [11, 10], the aerodynamic impact on the trailing wing in formation is relatively less responsive in the longitudinal separation, compared to the lateral spacing and vertical offset. To investigate the effects of vortex surfing in different lateral and vertical spacing, the trailing wing is placed at a matrix plane of various *y/b* and *z/b* coordinates, as illustrated in Figure 13. The study is carried out at longitudinal separation of *x/b* = 2, which is equivalent to the farthest plane in validation, *x/c* = 3.

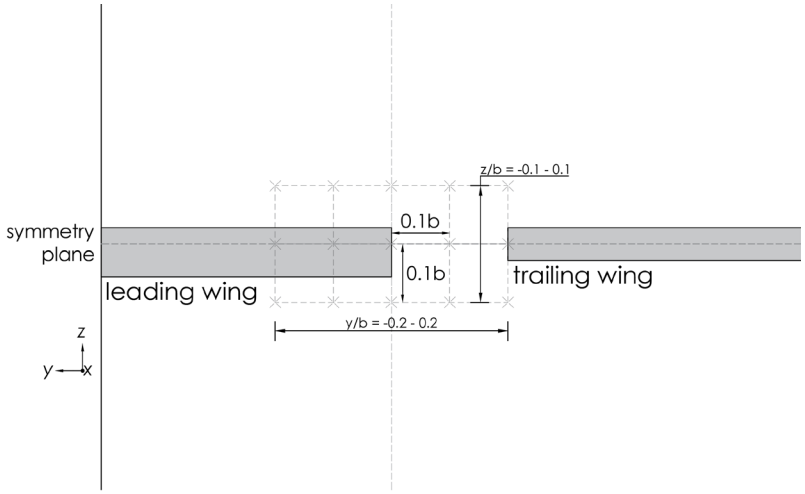

Figure 13. Lateral and vertical spacing for the leading-trailing wing.

The aerodynamic results of the trailing wing in wake surfing effect are shown in Figure 14. Across the lateral spacing, the trailing wing is undergoing different magnitude of vortex strength. As vortex core center is at about 0.1*c* inboard of the leading wingtip, any region beyond this point is considered as inverse effect.

The pressure contour on the trailing wing surface in formation along *y*-axis are showed in Table 3, for better illustration on the aerodynamic interactions in formation flight. The wingtip of trailing wing at *y/b* = -0.2 is interfering with the wake vortex and the pressure distribution on the leading edge and lower surface has severely affected the lift and drag performance. At *y/b* = -0.1, only a small margin of the wingtip is affected but the pressure on the suction surface is of the strongest amongst all. As a result, it is observed in Figure 14 that the lift coefficient is maximum when the wingtip is overlapping by 10% of the span (*y/b* = -0.1) or aligned with the leading wing (*y/b* = 0), and it drops enormously when the lateral spacing goes *y/b* = -0.2. When the trailing wing is flying at the more outer region of vortex core (*y/b* > 0), the surfing effects has also reduced, by approximately 50% from *y/b* = 0 to *y/b* = 0.1.

The trailing wing is experiencing higher drag as the wingtip is moving either inboard or outboard from the vortex core. The reduction in drag is mainly due to the axial velocity deficit within the vortex core region induced by the leading wing. Hence the overall lift-to-drag ratio is optimized when the lateral spacing is *y/b* = -0.1, where the trailing wing is gaining additional lift and encountering the least drag. However, even at other lateral positions, the trailing wing is still receiving an overall upwash benefit from the wake vortex, as compared to solo flight.

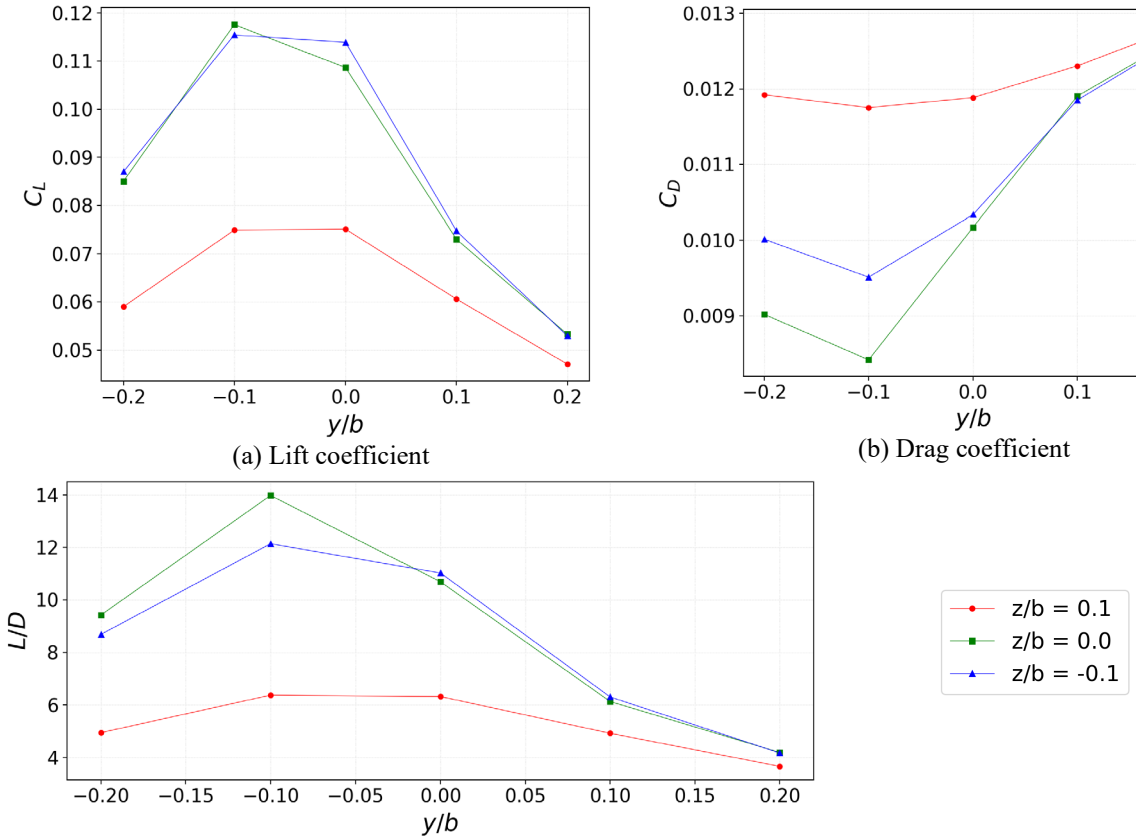

(a) Lift coefficient

(b) Drag coefficient

(c) Lift-to-drag ratio

Figure 14. Aerodynamics performance of trailing wing in different *y* and *z* positions at *x/b* = 2.

Table 3. Pressure contour on the trailing wing along *y*-axis, at *x/b* = 2, *z/b* = 0.

y/b	Lower surface	Wingtip and upper surface
-0.2	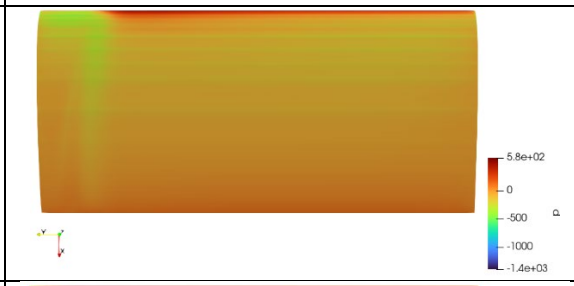	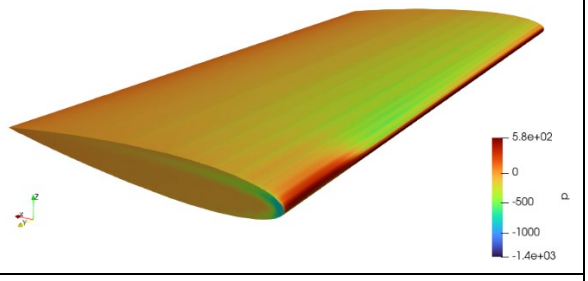
-0.1		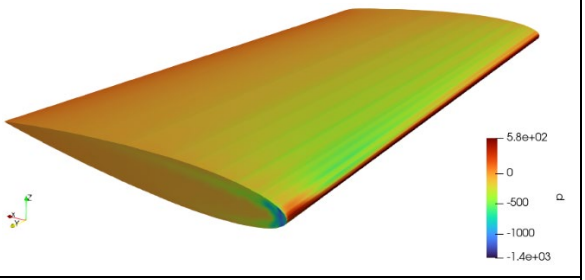
0		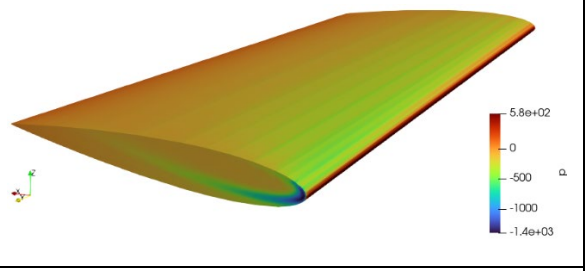
0.1		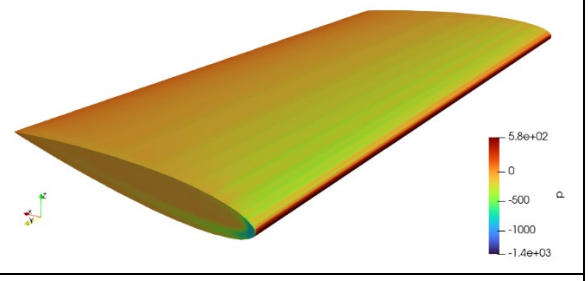
0.2		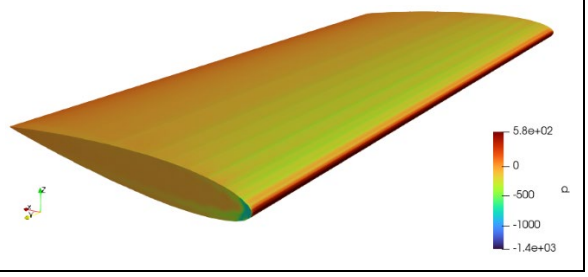

When it comes to vertical offset (*z/b*) in a formation flight, the level of both lift and drag coefficients are inferior when flying at a higher *z* position, irrelevant to the lateral spacing. As the lift is generated by the leading wing, the flow-field velocity in-between the wingtip vortices are pushing the airflow downwards [61], resulting in the downwards propagated wake vortices. Hence, trailing wing which fly above the waterline of leading wing is surfing on a weaker wake vortex and having less aerodynamic gains.

V. Conclusion

This paper has carried out the numerical simulation using both URANS and LES for vortex capturing, to validate the accuracy of the different turbulence models in predicting the aerodynamics of the wake vortices. The results showed that the LES model is more accurate in anticipating the wake vortex strength and persistence and provide a better agreement with the experimental data. URANS has achieved some degree of accuracy in estimating the vortex core center location and axial velocity deficit, but unable to maintain the vortex physics, and the vortices diffused more quickly than the reported data from experiment. Thus, for the trailing wing or aircraft to be 'surfing' on the properly modelled wake vortex, the authors recommended adopting the validated LES framework for the formation flight modelling.

For the formation flight simulation, the aerodynamic forces on both leading and trailing wing were examined, and the effects of the trailing wing positioning were investigated. In general, the aerodynamic properties of the leading wing are not affected by the formation, even with a tight longitudinal separation of $x/b = 1$. In contrast, the trailing wing flies in the updraft region of the wake is benefiting from the formation with higher lift and yet lower drag. As the vortex dynamics is relatively consistent in the near field, the aerodynamic impacts on the trailing wing are not much affected by the longitudinal separation. Nevertheless, the aerodynamic of trailing wing is more susceptible to the lateral and vertical spacing. The optimal position with the resolution in this study is at $y/b = -0.1$ and $z/b = 0$, which has obtained a lift-to-drag ratio of about 14. As the trailing wing moving further away from the vortex core, it reduced the aerodynamic interactions and hence lesser gains. This optimal position may be altered slightly if more simulation is run with finer resolution in the formation spacing.

The current study is focused on the close formation in the near field. Future research may look at a more efficient methodology for modelling the wingtip vortices evolution in the far field, which is applicable to the extended formation where the industry is more interesting in.

Acknowledgments

The work is part of the Industrial Postgraduate Programme co-funded by the Economic Development Board of Singapore and ST Engineering Aerospace Ltd.

References

[1] Airbus, "Airbus Global Market Forecast 2021- 2040," 13 November 2021. [Online]. Available: https://aircraft.airbus.com/sites/g/files/jlcbta126/files/2021-11/Airbus%20Global%20Market%20Forecast%202021-2040.pdf. [Accessed 03 Mar 2022].

[2] Boeing, "Commercial Market Outlook 2021 - 2040," 2022. [Online]. Available: https://www.boeing.com/resources/boeingdotcom/market/assets/downloads/CMO-2022-Report_FINAL_v01.pdf. [Accessed 05 August 2022].

[3] B. Graver, K. Zhang and D. Rutherford, "CO2 emissions from commercial aviation, 2018," The International Council on Clean Transportation , 2019.

[4] I. Abrantes, A. F. Ferreira, A. Silva and M. Costa, "Sustainable aviation fuels and imminent technologies - CO2 emissions evolution towards 2050," *Journal of Cleaner Production,* no. 313, 2021.

[5] R. Huang, M. Riddle, D. Graziano, J. Warren, S. Das, S. Numbalkar, J. Cresko and E. Masanet, "Energy and emissions saving potential of additive manufacturing: the case of lightweight aircraft components," *Journal of Cleaner Production,* no. 135, pp. 1559-1570, 2016.

[6] L. M. Dray, A. W. Schafer and K. A. Zayat, "The global potential for CO2 emissions reduction from jet engine passenger aircraft," *Transportation Research Record,* vol. 2672, no. 23, pp. 40-51, 2018.

[7] Y. D. Ko, Y. J. Jang and D. Y. Kim, "Strategic airline operation considering the carbon constrained air transport industry," *Journal of Air Transport Management,* no. 62, pp. 1-9, 2017.

[8] Y. Zhao, H. Wu, Q. Zhang and Q. Cheng, "Overview of surfing aircraft vortices for energy," *Journal of Physics: Conference Series (The 11th Asia Conference on Mechanical and Aerospace Engineering ACMAE),* vol. 1786, no. 1, pp. 12-26, 2021.

[9] W. B. Blake, S. R. Bieniawski and T. C. Flanzer, "Surfing aircraft vortices for energy," *The Journal of Defense Modeling and Simulation: Applications, Methodology, Technology,* vol. 12, no. 1, pp. 31-39, 2013.

[10] D. Hummel, "Aerodynamic aspects of formation flight in birds," *Journal of Theoretical Biology,* vol. 104, no. 3, pp. 321-347, 1983.

[11] D. Hummel, "Formation flight as an energy-saving mechanism," *Israel Journal of Zoology,* vol. 41, no. 3, pp. 261-278, 1995.

[12] E. C. Mills, T. K. Speer and J. L. Tate, "Formation Flight Technology," *Aircraft Engineering and Aerospace Technology,* vol. 43, no. 7, pp. 4-8, 1970.

[13] L. R. Jenkinson, R. E. Caves and D. P. Rhodes, "Automatic formation flight - A preliminary investigation into the application to civil operations," *Aircraft Engineering, Technology, and Operations Congress,* 1995.

[14] D. Fleischmann and M. M. Lone, "Analysis of wake surfing benefits using a fast unsteady vortex lattice method," *AIAA Scitech 2019 Forum,* 2019.

[15] D. Hummel, "The Use of Aircraft Wakes to Achieve Power Reductions in Formation Flight," in *Advisory Group for Aerospace Research & Development Fluid Dynamics Panel (AGARD FDP)*, Trondheim, Norway, 1996.

[16] M. J. Vachon, R. J. Ray, K. R. Walsh and K. Ennix, "F/A-18 Performance Benefits Measured During the Autonomous Formation Flight Project," NASA Drydan Flight Research Center, Edwards, California, 2003.

[17] E. Wagner, "An Analytical Study of T-38 Drag Reduction in Tight Formation Flight," Master Thesis, Department of The Air Force, Air University, Air Force Institute of Technology, Wright-Patterson Air Force Base, Ohio, 2002.

[18] E. Wagner, D. Jacques, W. Blake and M. Pachter, "Flight Test Results of Close Formation Flight for Fuel Savings," *AIAA Atmospheric Flight Mechanics Conference and Exhibit,* 2002.

[19] J. Pahle, D. Berger, M. Venti, C. Duggan, J. Faber and K. Cardinal, "An Initial Flight Investigation of Formation Flight for Drag Reduction on the C-17 Aircraft," *AIAA Atmospheric Flight Mechanics Conference,* 2012.

[20] S. R. Bieniawski, R. W. Clark, S. E. Rosenzweig and W. B. Blake, "Summary of Flight Testing and Results for the Formation Flight for Aerodynamic Benefit Program," *AIAA SciTech Forum 52nd Aerospace Science Meeting,* 2014.

[21] T. C. Flanzer and S. R. Bieniawski, "Operational Analysis for the Formation Flight for Aerodynamic Benefit Program," in *AIAA SciTech 52nd Aerospace Sciences Meeting*, Maryland, 2014.

[22] Airbus, "Airbus joined by European partners to demonstrate reduced emission fello'fly operations," 9 September 2020. [Online]. Available: https://www.airbus.com/sites/g/files/jlcbta136/files/d71469db351c7374f2eb9a0faa20da6e_Airbus-joined-by-partners-to-demonstrate-reduced-emission-fellowfly-operations.pdf. [Accessed 20 May 2022].

[23] Airbus , "fello'fly Wake Energy Retrieval Concept of Operations," August 2021. [Online]. Available: https://flipbook.mms-airbus.com/fellofly/index.html#/page/0. [Accessed 20 May 2022].

[24] Airbus, "Airbus joined by European partners to demonstrate reduced emission fello'fly operations," 9 September 2020. [Online]. Available: https://www.airbus.com/sites/g/files/jlcbta136/files/d71469db351c7374f2eb9a0faa20da6e_Airbus-joined-by-partners-to-demonstrate-reduced-emission-fellowfly-operations.pdf. [Accessed 31 May 2020].

[25] D. J. Halaas, S. R. Bieniswski, B. Whitehead and W. B. Blake, "Formation Flight for Aerodynamic Benefit Simulation Development and Validation," *52nd Aerospace Sciences Meeting,* 2014.

[26] D. Singh, A. F. Antoniadis, P. Tsoutsanis, H.-S. Shin, A. Tsourdos, S. Mathekga and K. W. Jenkins, "A Multi-Fidelity Approach for Aerodynamic," *Aerospace,* vol. 5, no. 2, p. 66, 2018.

[27] D. Zhang, Y. Chen, X. Dong, Z. Liu and Y. Zhou, "Numerical Aerodynamic Characteristics Analysis of the Close Formation Flight," *Mathematical Problems in Engineering,* pp. 1-13, 2018.

[28] D. Vechtel, D. Fischenberg and J. Schwithal, "Flight dynamics simulation of formation flight for energy saving using LES-generated wake flow fields," *CEAS Aeronautical Journal,* vol. 9, no. 4, pp. 735-746, 2018.

[29] R. H. Bush, T. Chyczewsky, K. Duraisamy, B. Eisfeld, C. L. Rumsey and B. R. Smith, "Recommendations for Future Efforts in RANS Modeling and Simulation," *AIAA SciTech Forum,* 2019.

[30] C. H. Moeng and P. P. Sullivan, Large-Eddy Simulation, National Center for Atmospheric Research, Boulder, CO, USA, 2015.

[31] B. Chaouat, "The State of Art of Hybrid RANS/LES Modeling for the Simulation of Turbulent Flows," *Springer Science+Business Media,* pp. 279-327, 2017.

[32] W. F. Philips, Mechanics of Flight, John Wiley & Sons Ltd, 2009.

[33] A. Bakker, L. Oshionowa and A. Haidari, "Realize greater benefits from CFD," *Chemical Engineering Progress,* 2001.

[34] OpenFOAM, "OpenFOAM," n.d.. [Online]. Available: https://www.openfoam.com/. [Accessed 07 May 2022].

[35] B. K. J. Tan , P. C. Wang and S. Srigrarom, "Computational Modelling of Wing Downwash Profile with Reynolds-Averaged and Delayed Detached-Eddy Simulations," in *23rd AIAA Computational Fluid Dynamics Conference*, Denver, Colorado, 2017.

[36] B. K. J. Tan, H. Hesse and P. C. Wang, "Numerical Capture and Validation of a Massively Separated Bluff-Body Wake," in *AIAA AVIATION 2020 FORUM*, Virtual Event, 2020.

[37] M. S. O'Regan, P. C. Griffin and T. M. Young, "A vorticity confinement model applied to URANS and LES simulations of a wing-tip vortex in the near-field," *International Journal of Hear and Fluid Flow,* vol. 61, no. 2016, pp. 355-365, 2016.

[38] T. Snyder and M. Braun, "Comparison of Perturbed Reynolds Equation and CFD Models for the Prediction of Dynamic Coefficients of Sliding Bearings," *Lubricants,* vol. 6, no. 1, p. 5, 2018.

[39] C. Greenshields, "5.3 Mesh generation with the blockMesh utility," CFD Direct, 12 July 2022. [Online]. Available: https://doc.cfd.direct/openfoam/user-guide-v10/blockmesh.

[40] C. Greenshields, "OpenFOAM v10 User Guide - 5.4 Mesh generation with the snappyHexMesh utility," CFD Direct, 12 July 2022. [Online]. Available: https://doc.cfd.direct/openfoam/user-guide-v10/snappyhexmesh.

[41] T. A. Smith and Y. Ventikos, "Wing-tip vortex dynamics at moderate Reynolds unmbers," *Physics of Fluids,* no. 33, 2021.

[42] C. Greenshields, "OpenFOAM v10 User Guide - 3.6 Standard utilities," CFD Direct, 12 July 2022. [Online]. Available: https://doc.cfd.direct/openfoam/user-guide-v10/standard-solvers.

[43] A. Dewan, Tackling Turbulent Flows in Engineering, New Delhi: Springer, 2011.

[44] K.-S. Yang and J. H. Ferziger, "Large-Eddy Simulation of Turbulent Obstacle Flow Using a Dynamic Subgrid-Scale Model," *AIAA Journal,* vol. 31, no. 8, pp. 1406-1413, 1993.

[45] F. R. Menter, "Zonal two equation k-ω turbulence models for aerodynamics flows," in *24th Fluid Dynamics Conference*, Orlando, 1993.

[46] A. J. Menter, "Two-equation eddy-viscosity turbulence models for engineering applications," *AIAA Journal,* vol. 32, no. 8, pp. 1598-1605, 1994.

[47] N. N. Ahmad, "Numerical Simulation of the Aircraft Wake Vortex Flowfield," in *5th AIAA Atmospheric and Space Environments Conference*, San Diego, CA, 2013.

[48] M. S. O'Regan, P. C. Griffin and T. M. Young, "Numerical and experimental investigation of the mean and turbulent characteristics of a wing-tip vortex in the near field," *Journal of Aerospace Engineering,* vol. 228, no. 13, pp. 2516-2529, 2014.

[49] R. Lohner, "On limiters for minimal vorticity dissipation," in *47th AIAA Aerospace Sciences Meeting Including The New Horizons Forum and Aerospace Exposition*, Orlando, 2009.

[50] D. Kolomenskiy, R. Paoli and J.-F. Boussuge, "Hybrid RANS-LES simulation of wingtip vortex dynamics," in *Proceedings of the ASME 2014 4th Joint US-European Fluids Engineering Division Summer Meeting* , Chicago, 2014.

[51] F. Rezaei, E. Roohi and M. Pasandideh-Fard, "Stall simulation of flow around an airfoil using LES model and comparison of RANS models at low angles of attack," in *15th Conference On Fluid Dynamics*, Bandar Abbas, Iran, 2013.

[52] J. Smagorinsky, "General circulation experiments with the primitive equations," *Monthly Weather Review,* vol. 91, no. 3, pp. 99-164, 1963.

[53] D. Carati, G. S. Winckelmans and H. Jeanmart, "On the modelling of the subgrid-scale and filtered-scale stress tensors in large-eddy simulation," *Journal of Fluid Mechanics,* vol. 441, pp. 119-138, 2001.

[54] "ParaView," kitware, 2022. [Online]. Available: https://www.paraview.org/.

[55] S. Ragab and M. Sreedhar, "Numerical simulation of vortices with axial velocity deficits," *Physics of Fluids,* no. 7, pp. 549-558, 1995.

[56] S. Ragab and M. Screedhar, "Numerical simulation of vortices with axial velocity deficits," *Physics of Fluids,* no. 7, pp. 549-558, 1995.

[57] S. Martínez-Aranda, A. L. García-González, L. Parras, J. F. Velázquez-Navarro and C. del Pino, "Comparison of the Aerodynamic Characteristics of the NACA0012 Airfoil at Low-to-Moderate Reynolds Numbers for any Aspect Ratio," *International Journal of Aerospace Sciences,* vol. 4, no. 1, pp. 1-8, 2016.

[58] A. Shekarriz, T. C. Fu and J. Katz, "Near-field behavior of a tip vortex," *AIAA Journal,* vol. 31, no. 1, 1993.

[59] M. Munk, The minimum induced drag of Aerofoils, Technical Report Archive & Image Library, 1923.

[60] P. B. S. Lissaman and C. A. Shollenberger, "Formation Flight of Birds," *Journal of Science,* vol. 168, no. 3934, pp. 1003-1005, 1970.

[61] C. Breitsamter, "Wake vortex characteristics of transport aircraft," *Progress in Aerospace Sciences,* vol. 47, no. 2, pp. 89-134, 2011.